Night-time chemistry of biomass burning emissions in urban areas: A dual mobile chamber study

Spiro D. Jorga[1], Kalliopi Florou[2], Christos Kaltsonoudis[2], John K. Kodros[2], Christina Vasilakopoulou[2,3], Manuela Cirtog[5], Axel Fouqueau[6], Bénédicte Picquet-Varrault[5], Athanasios Nenes[2,4], and Spyros N. Pandis[1,2,3]

[1]Department of Chemical Engineering, Carnegie Mellon University, Pittsburgh, 15213, USA

[2]Institute of Chemical Engineering Sciences, ICE-HT, Patras, 26504, Greece

[3]Department of Chemical Engineering, University of Patras, Patras, 26504, Greece

[4]School of Architecture, Civil & Environmental Engineering, Ecole Polytechnique Federale de Lausanne, Lausanne, 1015, Switzerland

[5]LISA, UMR CNRS 7583, Université Paris-Est Créteil, Université de Paris, Institut Pierre Simon Laplace (IPSL), Créteil, France

[6]Laboratoire National de Métrologie et d'Essais (LNE), 75015 Paris, France

Correspondence to: Spyros N. Pandis (spyros@chemeng.upatras.gr)

Abstract.

Residential biomass burning for heating purposes is an important source of air pollutants during winter. Here we test the hypothesis that significant secondary organic aerosol production can take place even during winter nights through oxidation of the emitted organic vapors by the nitrate (NO_3) radical produced during the reaction of ozone and nitrogen oxides. We use a mobile dual smog chamber system which allows the study of chemical aging of ambient air against a control reference. Ambient urban air sampled during a wintertime campaign during night-time periods with high concentrations of biomass burning ~~organic aerosol~~emissions was used as the starting point of the aging experiments. Biomass burning organic aerosol (OA) was on average 70% of the total OA in the beginning of our experiments. Ozone was added in the perturbed chamber to simulate mixing with background air (and subsequent NO_3 radical production and aging), while the second chamber was used as a reference. Following the injection of ozone, rapid ~~organic aerosol (~~OA~~)~~ formation was observed in all experiments leading to increases of the OA concentration by 20-70%. The oxygen-to-carbon ratio of the OA increased on average by 50% and the mass spectra of the produced OA was quite similar to the oxidized OA mass spectra reported during winter in urban areas. Further, good correlation was found for the OA mass spectra between the ambient-derived emissions in this study and the nocturnal aged laboratory-derived biomass

33 burning emissions from previous work. Concentrations of NO_3 radicals as high as 25 ppt were
34 measured in the perturbed chamber with an accompanying production of 0.1-3.2 μg m^{-3} of organic
35 nitrate in the aerosol phase. Organic nitrate represented approximately 10% of the mass of the
36 secondary OA formed. ~~The organic nitrate fraction to the total OA formed was on average 10%.~~
37 These results strongly indicate that the OA in biomass burning plumes can chemically evolve
38 rapidly even during wintertime periods with low photochemical activity.
39
1. Introduction

41   Biomass burning from residential heating, agricultural fires, prescribed burning, and
42 wildfires is a major source of atmospheric pollutants worldwide (Watson 2002, Bond et al. 2004,
43 Robinson et al. 2006). Emissions from biomass burning contribute both primary organic aerosol
44 (POA) and organic vapors that upon further reactions in the atmosphere can produce secondary
45 organic aerosol (SOA) (Andreae & Merlet 2001, Akagi et al., 2011, Bruns et al., 2016, Akherati
46 et al., 2020). The use of wood burning for domestic heating purposes is one of the major sources
47 of OA in many countries and is a major contributor to the violation of daily PM standards in
48 European cities (Alfarra et al., 2007, Favez et al., 2010, Fuller et al., 2014). Biomass burning
49 emissions and their products have significant but still uncertain impacts on human health and
50 climate (Ford et al., 2018; O'Dell et al., 2019).

51   The organic aerosol emitted during biomass burning undergoes extensive physical and
52 chemical changes in the atmosphere. More volatile components evaporate as emissions dilute in
53 the atmosphere (Tkacik et al., 2017); these semivolatile organic compounds (SVOCs) together
54 with the other emitted intermediate volatility (IVOCs) and volatile organic compounds (VOCs)
55 are subsequently oxidized leading to the production of SOA. Photochemical oxidation of biomass
56 burning emissions and the resulting SOA production have been studied both in the laboratory
57 (Hennigan et al., 2011; Ortega et al., 2013; Tkacik et al., 2017; Ahern et al.; 2019; Kodros et al.,
58 2020) and in the field (Capes et al., 2008; Jolleys et al., 2015; Vakkari et al., 2018). The reactions
59 of VOCs, IVOCs and SVOCs with the OH radical are considered to be the dominant chemical
60 pathway for oxidation, but reactions of emitted monoterpenes with ozone can also contribute to
61 the SOA formation during the chemical aging of biomass burning emissions (Yu et al., 1999, Zhao
62 et al., 2015). Despite considerable uncertainties remaining on the amount of SOA that can be
63 produced, and the net change of the biomass burning OA concentration when evaporation is

64 considered, it is clear that this daytime processing is important for converting the fresh biomass

65 burning OA to oxidized OA (OOA) (Bougiatioti et al., 2014).

66 Atmospheric processing of biomass burning OA during periods of low photochemical

67 activity (such as in winter or at night), known also as "dark" aging, has received substantially less

68 attention than photochemical processing. Recent aircraft measurements during agricultural

69 biomass burning periods indicated that nighttime oxidation of biomass burning VOCs is dominated

70 by NO_3 (Decker et al., 2019). Hartikainen et al. (2018) reported high amounts of nitrogen-

71 containing organic compounds both in the gas and particle phase after dark aging of residential

72 wood combustion emissions. Kodros et al. (2020) reported significant and rapid OOA production

73 in laboratory experiments in which fresh biomass burning emissions were exposed to NO_3 and

74 suggested that dark oxidation may be an important process on regional scales. In the same study,

75 ambient measurements in an urban area suggested that the mixing of O_3 from the residual layer

76 down to the nocturnal boundary layer can enhance the formation of NO_3 and the nighttime

77 oxidation of biomass burning emissions. The mixing of ozone from the residual layer and the

78 importance to nightime chemistry was also suggested in studies on nightime oxidation of biogenic

79 VOCs (Brown et al., 2009; Brown et al., 2013). Despite this important finding, the degree to which

80 biomass burning plumes undergo night-time aging and produce significant amounts of SOA

81 remains poorly understood. Lacking consideration of such nocturnal chemistry in transport models

82 has been suggested as a possible source of the under prediction oxidized organic aerosol mass by

83 a factor of 3-5 (Fountoukis et al., 2016; Tsimpidi et al., 2014) during wintertime in polluted areas

84 with low photochemical activity.

85 Usually smog chamber studies use fresh biomass burning emissions generated in the

86 laboratory by a single source ~~with many cases using clean air~~ as a starting point of their

87 experiments. The use of a dual chamber system with starting point ambient air rich in biomass

88 burning emissions but also primary and secondary pollutants from other sources offers a bridge

89 between ~~the~~ traditional laboratory studies and ~~the~~ ambient observations.~~.~~ ~~The use of the dual~~

90 ~~chamber~~Such a system offers the capability of aging realistic biomass burning emissions from

91 multiple sources and fuels, diluted in the atmosphere and mixed with other pollutants (e.g., NO_x

92 from transportation)~~. It therefore offers a bridge between laboratory experiments and ambient~~

93 ~~observations.~~ In this study, we take advantage of the high levels of OA from residential biomass

94 burning in Patras, Greece (the country's third-largest city), to investigate the importance of night-

95   time chemistry in the processing of biomass burning OA. Biomass burning leads to concentrations

96   of OA exceeding 50 µg m^{-3} in Patras in the early evening (Florou et al., 2017). A dual atmospheric

97   simulation chamber system is used to elucidate the formation of SOA during winter periods in

98   urban areas with high biomass burning organic aerosol concentrations. ~~Usually chamber studies~~

99   ~~use fresh biomass burning emissions generated in the laboratory. The use of the dual chamber~~

100 ~~system offers the capability of aging realistic biomass burning emissions mixed with other~~

101 ~~pollutants. It therefore offers a bridge between laboratory experiments and ambient observations.~~

102

103 **2. Experimental Methods**

104 **2.1 Dual chamber system**

105   The dual chamber system developed by Kaltsonoudis et al. (2019) was used for

106 experiments in early 2020 in Patras, Greece during the PyroTRACH-PANACEA Wintertime 2020

107 experiment. The system consists of two 1.5 m^3 Teflon (PTFE) reactors attached to metallic frames.

108 Use of the second reactor as a reference (control chamber) allows the identification and potential

109 correction for any major experimental artifacts that could be due to the walls of the chamber and

110 the other complexities of this experimental system. The dual chamber system was deployed from

111 January 10 till February 15, 2020 in the city of Patras. The chambers along with the available

112 instrumentation were located indoors, in the campus of the University of Peloponnese,

113 approximately a few kilometers away from the center of the city (Figure S1). The windows of the

114 laboratory were kept open before and during the experiments, so the temperature of the dual

115 chamber system was in the~~ranging from~~ 12-20°C range, while the outdoor temperature was on

116 average 5 degrees lower. The relative humidity (RH) in the chambers ranged from 35 to 45% ~~only~~

117 ~~a few degrees higher than that of the outdoor environment.~~.

118

119 **2.2 Experimental description**

120   Both chambers were flushed with ambient air before each experiment using a metal bellows

121 pump (Senior Aerospace, MB-602) for 1-2 h. This process is used to achieve higher sampling

122 efficiency and brings the system (chamber walls, tubing) close to equilibrium with ambient air

123 reducing losses of vapors to the sampling lines and walls of the chamber. Ambient air during

124 nighttime cold periods was introduced inside both chambers. In one of the chambers, (perturbed

125 chamber) ozone was added and upon reaction with the existing NO$_x$ in the chamber formed NO$_3$

126   radicals. The second chamber (control chamber) was used as the reference in order to help us

127   understand the unperturbed evolution of the system inside the chamber. During all experiments

128   the chambers were under dark conditions. Ambient air was flushed through each of the chambers

129   with a flow of 80 L min^{-1}. More than 70% of the ambient PM was transferred to the chambers and

130   the concentrations of the measured VOCs were within 5% of their ambient values.

131   Using an automated valve switching between the two reactors, the particle and gas

132   concentrations in both chambers were measured. Data were collected 1.5 min after the switching

133   of the valve to avoid any memory effects related to the sampling lines. For the gas phase

134   measurements PTFE tubing (0.25 in) was used, while for the particle phase the tubing was copper

135   (0.25 in).

136   After filling the chambers with ambient air, the content of each chamber was characterized

137   for approximately one hour. The ozone added in the perturbed chamber after the characterization

138   period was in the range of 50-250 ppb. These values are higher than the 20 ppb measured during

139   the nighttime in Patras in this campaign, but some acceleration of the corresponding chemical

140   processes is necessary to reduce the effects of the walls and to limit the duration of the experiments

141   in the relatively small chambers used.

142   In selected experiments, approximately 40 ppb of d9-butanol was added in both chambers

143   to measure the OH concentration. Following Barnet et al. (2012), the OH concentration in the

144   chambers was estimated with the measured decay of the butanol concentration assuming a reaction

145   rate constant with OH of 3.4×10^{12} cm^3 molecule^{-1} s^{-1}.

146   An incoherent broad-band cavity-enhanced absorption spectroscopy (IBB-CEAS) was

147   used to measure the NO$_3$ radical concentration. Detailed information about the technique can be

148   found elsewhere (Venables et al., 2006; Ventrillard-Courtillot et al., 2010; Chen and Venables,

149   2011; Fouqueau et al., 2020). Briefly the light from a LED source centered on the 662 nm

150   absorption cross section of NO$_3$ radical is focused and introduced into a high-finesse optical cavity

151   composed of two high reflectivity (~99.98%) and 1 m curvature mirrors. The optical cavity has a

152   length of 0.61 m and allows up to 4.5 km (at 662 nm) optical path and a detection limit up to 3 ppt

153   (integration time of 10 seconds). Particle-free air is passed through the cavity at 2.5 L min^{-1}.

154   Spectra between 640 and 685 nm were recorded with an OceanOptics QE-65 Pro spectrometer. A

155   time resolution of one minute was selected for these experiments. Calibration with NO$_2$ (800 ppb

156   in dry nitrogen, Air Liquide) was performed daily in order to precisely determine the reflectivity

157 of the mirrors and estimate the optical path. The sample spectra were fitted against standard spectra

158 of gas species absorbing in the spectral region of the instrument: NO_3 radical (Orphal et al., 2003),

159 NO_2 (Vandaele et al., 1998) and H_2O (reference spectrum recorded with the instrument) using the

160 DOASIS software.

161 A quadrupole proton-transfer reaction mass spectrometer (PTR-MS, Ionicon Analytik) was

162 used to measure the concentration of VOCs including d9-butanol. We calculated the initial VOC

163 levels in the chambers using the concentrations of m/z 42 (acetonitrile), 69 (isoprene), 71 (MVK

164 & MACR), 73 (MEK), 79 (benzene), 93 (toluene) and 107 (xylene). We used the above m/z peaks,

165 because the PTR-MS was calibrated for those values. For the experiments that the PTR-MS was

166 not available we scaled the initial VOCs concentration using the black carbon (BC) levels. Using

167 a series of gas monitors the concentration of nitrogen oxides (NO and NO_2) and ozone (O_3) were

168 measured (Teledyne models: T201 and 400E respectively).

169 A TSI scanning mobility particle sizer (SMPS, classifier model 3080; DMA model 3081

170 CPC model 3775) was used for measuring the particle number distribution in the 15-700 nm range.

171 An Aerodyne high-resolution time-of-flight aerosol mass spectrometer (HR-ToF-AMS) was

172 measuring the composition and mass spectrum of OA. We did not use a dryer before the

173 instruments and the RH of the samples was recorded. For the analysis of the HR-ToF-AMS data

174 we used the AMS software toolkit (SQUIRREL v1.57I) and for the high-resolution data the Peak

175 Integration by Key Analysis (PIKA v1.16I) software. The elemental ratios were calculated using

176 the improved method of Canagaratna et al. (2015). The mass concentration and particle distribution

177 of black carbon (BC) were measured using a single-particle soot photometer (SP2, Droplet

178 Measurement Techniques).

179 The collection efficiency (CE) of the AMS was calculated applying the algorithm of

180 Kostenidou et al. (2007), comparing the SMPS volume distributions and the AMS mass

181 distributions. The CE ranged between 0.40-0.45 depending on the experiment. Using the same

182 algorithm, the density of the OA was calculated to be in the range of 1.25-1.4 g cm^{-3}.

183 Using the theta (θ) angle (Kostenidou et al., 2009) a comparison between the OA spectra

184 of the ambient and the chamber content after filling, we concluded that the OA composition

185 injected in the chambers was the same as in the ambient air. The theta angle between the two

186 chambers and the ambient OA spectra was always less than 4 degrees, suggesting excellent

187 agreement. Also, the OA mass spectra in the two chambers right after their filling was in very good

agreement (θ=3-4°), confirming that both chambers had the same OA composition initially. The thetaθ angle is a useful metric for the comparison of OA mass spectra, similar to the often used R^2. A θ theta angle for theof two AMS spectra ranging fromin the 0-5° range indicates an excellent match between the compared spectra, which should be considered identical for all practical purposes (R^2 ranging from 1 to -0.99). For a θ angle of 6-10° there is a good match (R^2 approximately 0.98-0.96), but there are some small differences. A θ of 11-15° shows that the spectra are quite similar, but they are not the same (R^2: 0.95-0.92), while for a θ in the 16-30° range the spectra ares coming from different sources, but there are some similarities (R^2: 0.91-0.73). A θ theta angle higher than 30° suggests clearly different AMS spectra. We use the θ theta angle in this study due to its ability to better represent relatively smalller differences than the coefficient of determination.

Following the completion of each perturbation experiment, a wall-loss characterization experiment was conducted to measure the size-dependent particle wall-loss rate constant inside the two chambers (Wang et al., 2018). The particles were produced by the atomization (TSI, model 3076) of an aqueous solution of ammonium sulfate (5 g L^{-1}). and subsequent diffusion drying and were injected into both chambers. The ammonium sulfate seeds after the atomizer passed through a diffusion dryer and then were injected in the chambers without passing through a neutralizer. . We did not use a neutralizer after the atomizer. Using an ionizing fan, the chamber walls were swept before the start of each experiment to keep the particle loss rates low (Jorga et al., 2020).

The perturbation experiments started around 18:0017:30-18:300 LT each evening (approximately 30 min after the sunset which during the campaign was from 17:010 to -18:00 LT), when the OA concentration was elevated from local nocturnal biomass burning emissions in the area for heating. The initial conditions in the experiments are summarized in Table 1. Thirteen experiments, eleven involving perturbation and two blank experiments, in which no ozone was injected in either chamber, were performed during January and February 2020 using ambient air from Patras.

3. Results of a Typical Perturbation Experiment

218   Our study ~~has been~~was designed so that the experiments would start when biomass burning
219   was~~is~~ the major source of both organic aerosol and VOCs. In this section we first present in detail
220   the results of one typical experiment~~s~~ (Exp. 1) and then we ~~with more details before~~ summarize~~ing~~
221   the results of the rest of the conducted experiments.
222
223   **3.1 Results of a typical perturbation experiment**
224   The average PM_1 concentration in the chambers during the filling process of Exp. 1 was
225   approximately 50 μg m^{-3}. The concentration of OA during that period was 44 μg m^{-3} with 2.4 μg
226   m^{-3} of BC. The positive matrix factorization (PMF) analysis of the full campaign ambient data set
227   suggested that 70% of the OA at the time of filling originated from biomass burning. Other OA
228   sources included cooking OA or COA (15%), oxygenated OA or OOA (10%) and hydrocarbon-
229   like OA or HOA (5%). PMF was applied to the high resolution AMS organic mass spectra (m/z
230   up to 300) at 3 min resolution from the month long field campaign. ~~Using a 3 minute resolution~~
231   ~~PMF~~Solutions with ~~with~~ one to seven factors were investigated. The best solution
232   included~~resulted in~~ 4 factors corresponding to ~~included one~~BBOA, ~~factor an~~OOA, ~~a~~COA and~~a~~
233   HOA. The ~~Figure S2 represents the~~ time series of the four factors ~~identified~~ during the full~~ield~~
234   field campaign are shown in Figure S2. The ~~with~~ detailed analysis of the field campaign, the
235   determination of the PMF factors as well as particle and gas measurements will be included in a
236   forthcoming publication.
237   The initial concentration of O_3 in the two chambers was 10 ppb, of NO 17 ppb and of NO_2
238   24 ppb, values within 5% of their ambient concentrations. The measured initial VOC levels were
239   approximately 150 μg m^{-3} while the RH inside ~~the~~ both chambers was approximately 45%.~~.~~ The
240   rest of the conditions are summarized in Table 1.
241   In Exp.1 NO_2 increased to 30 ppb in the perturbed chamber in approximately 30 min after
242   the ozone injection while at the same time NO levels dropped to close to zero. In the perturbed
243   chamber 2 hours after the injection the mixing ratio of NO_2 was 18 ppb and of ozone 220 ppb. In
244   the control chamber the concentrations of the above mentioned gases remained within 10% of their
245   initial levels. Due to the time needed for mixing and the rapid reaction of NO and O_3 it is difficult
246   to measure accurately the injected O_3 concentration. A zeroth order estimate can be made assuming
247   that the injected amount of ozone is equal to the final (equilibrated) amount of ozone in the

248 perturbed chamber plus the reacted NO_x (Table S1). Based on this zeroth order estimate, the

249 injected ozone in Exp. 1 was approximately 240 ppb.

250 Following the injection of ozone in the perturbed chamber (t=0 h) there was a rapid increase

251 of OA (~~Fig.~~Figure 1). Approximately 33 µg m^{-3} of SOA was produced in 2.5 hours (70% increase

252 from the initial injected OA levels). In just one hour after the injection of ozone, the OA

253 concentration increased by approximately 25 µg m^{-3}. This high rate secondary OA production rate

254 of approximately 25 µg m^{-3} h^{-1}is at least partially due to~~the result of~~ the high ozone levels used in

255 these experiments to accelerate the corresponding chemistry and reduce the problems caused by

256 losses of both particles and vapors to the walls of the chamber. ~~This roughly corresponds to an~~

257 ~~initial OA formation rate of 25 µg m^{-3} h^{-1}.~~,Although this formation rate is true under high ozone

258 levels, the absolute increase in the OA concentration ~~result~~ indicat~~ing~~es the strong potential of the

259 ambient air in an urban area with strong biomass burning emissions to form SOA even under dark

260 conditions. The change of OA in the control chamber after the particle wall-loss corrections was

261 less than 7% at all times. This strongly indicates that the OA changes in the perturbation chamber

262 were not due to experimental artifacts.

263 The sulfate concentration remained practically the same (within 10%) in both the perturbed

264 and the control chambers after accounting for particle wall-losses. The initial nitrate in the

265 perturbed chamber was 1 µg m^{-3} more than in the control. This small difference can be an artifact

266 of the sampling system in this specific experiment. Production of approximately 6 µg m^{-3} of aerosol

267 nitrate was observed in the perturbed chamber with the majority of this increase in the form of

268 organic nitrate. Using the method described in Farmer et al. (2010) using the NO^+/NO_2^+ ratio from

269 the AMS, we estimate that close to 60% of the formed secondary aerosol nitrate in the perturbed

270 chamber was organic nitrate. Taking into account the organic nitrate, there was a 77% increase of

271 the OA compared to the initial concentration.

272 An increase of the ammonium concentration by close to 1 µg m^{-3} was observed in the

273 perturbed chamber (a 90% increase of ammonium compared to its~~the~~ levels before the injection of

274 ozone) while in the control chamber its concentration remained within 8% of the initial value.

275 Most of this increase was due to the formation of ammonium nitrate. Approximately~~Almost~~ 4~~3~~0%

276 of the total nitrate formed was inorganic nitrate, which requires approximately 1 µg m^{-3} of

277 ammonium to be neutralized.~~,~~ So the increase in ammonium is consistent with the increase in

278 inorganic assuming that ammonium nitrate was formed. ~~suggesting that the increase in the~~

281

3.~~1~~ 2 Organic aerosol spectra

Figure 2 represents the OA mass spectra in the two chambers at the start and end of Exp.1. The c~~C~~omparison of~~ing~~ the OA mass spectra in the perturbed chamber at the beginning (after the air injection) and at the end (2.5 hours after the ozone injection) of Exp. 1 indicates that there was an increase in the fractional signal of m/z: 28 (CO^+), 29 (CHO^+), 30 (CH_2O^+), 43 ($C_2H_3O^+$), and 44 (CO_2^+). The highest decrease was observed in 55 ($C_4H_7^+$), 57 ($C_4H_9^+$), 60 ($C_2H_4O_2^+$), 69 ($C_5H_9^+$), 91 ($C_7H_7^+$) and 95 ($C_7H_{11}^+$). The theta angle between the spectra was 19 degrees, indicating significant change. The initial and final spectra in the control chamber had a θ angle of 8 degrees, with changes in m/z 28, 44, 57 and 60. ~~Figure 2 represents the OA mass spectra in the two chambers at the start and end of Exp. 1.~~

The O:C ratio ~~during Exp. 1~~ in the control chamber remained practically ~~the same~~ constant during Exp. 1, with a value close to 0.4 .~~increased slightly from 0.4 to 0.41 during the experiment~~ (~~Fig.~~Figure 3). This suggests that there was relatively low ~~but probably non-zero~~ chemical activity in this chamber. This is consistent with the small change in the OA mass spectrum. ~~-~~This activity is ~~probably~~could be due to the existing O_3 and any produced NO_3 in the control chamber. ~~although the NO₃ would react away faster.~~ ~~This activity is probably due to the O₃ that existed in this chamber.~~ On the contrary in the perturbed chamber after the injection of ozone the O:C ratio increased rapidly reaching 0.52 after 30 min. At the end of the experiment, the O:C ratio in the perturbed chamber reached a value of 0.61, similar to the measured ambient value around 3:00 LT at night.

To calculate the mass spectrum of the produced OA in the perturbed chamber, we used a simple mass balance approach. Details about this method can be found in Jorga et al. (2020). Concisely, assuming that the main processes in the chamber are losses of particles to the chamber walls and SOA formation, we estimate the initial (before the injection of ozone) and produced OA mass spectra. Using the size-dependent particle ~~rate loss~~loss rate constant measured at the end of each experiment, the concentration of the ~~pre-existing~~pre-existing OA as a function of time can be calculated. The pre-existing OA concentration in the perturbation chamber decreased from approximately 30 to 12 µg m^{-3} during Exp. 1 (Figure 4). Additional information about the particle

loss correction approach together with the size dependence of the particle loss rate constants for Exp. 1 (Figure S3)~~(can be found in the~~Check the SI ~~for details on this correction approach along with the profile of the particle loss rate constants in Figure S3)~~. The produced SOA that remains suspended in the chamber is then the difference between the total measured ~~OA~~ and the ~~initial~~ pre-existing or "initial" OA (Figure 4). The maximum concentration of the produced SOA was 23 μg m^{-3}, but it was gradually reduced to 15 μg m^{-3} due to the particle losses to the walls. With the concentrations of the pre-existing OA and the produced SOA both suspended in the chamber (these are the actual concentrations not corrected for wall losses) the AMS spectra that correspond to the sum of the two, the spectrum of the produced SOA can be estimated. ~~. Figure 4 and Figure 5 show the estimated produced OA and corresponding AMS mass spectrum in Exp. 1, respectively. Figure 4 is used to illustrate the concentrations of the OA components (primary and produced) during the corresponding experiment.~~ Figure 5 shows the resulting spectra for the produced SOA both for Exp. 1 and the average SOA spectra for all the experiments. The similarity of the spectra supports our choice of Exp. 1 as representative of the rest.~~Figure 4 shows the estimated produced OA in Exp. 1 and Figure 5 the corresponding AMS spectrum.~~

Our estimation of the~~The~~ produced SOA levels is based on the mass balance approach of Jorga et al. (2020) and not on the yields and concentration reduction of ~~the~~ individual VOCs. Given the uncertainties in the concentrations and the yields of the various VOCs and IVOCs in this complex~~e~~ system this is a more accurate estimate. We assume that the main process responsible for the reduction of the initial OA is loss of particles to the walls and that the loss of particle mass by evaporation and then loss of the vapors to the walls is negligible. The accuracy of this assumption can be confirmed by the change of the OA in the reference chamber (Figure 1a). The small change of the particle wall loss-corrected OA concentration (less than 7%) supports our assumption. If evaporation and vapor wall loss were important processes the corresponding concentration in the reference chamber would be decreasing significantly. ~~—~~This is one of the advantages of our approach using ambient air. The evaporation of the bbOA after its emission has already taken place in the atmosphere. Therefore, the SOA production that we measure does account for the SVOCs that have moved to the gas-phase as the bbOA gets diluted in the atmosphere. The changes in the reference chamber illustrate well the changes that continue to happen in the system without our acceleration of the chemistry.

The produced OA mass spectra from the perturbed chamber were compared with the produced OA factor from the dark aging of biomass burning emissions in the laboratory (Kodros et al., 2020). Although the present study deals with ~~ambient~~ emissions from multiple biomass burning sources and fuels in a ~~with more~~ complex air mixture and varying conditions compared to~~than~~ the laboratory work ~~that we are comparing with,~~ (that used specific biomass burning emissions under idealized conditions)~~,~~ a comparison can provide us with information about the consistency of the two studies. Kodros et al. (2020) performed chamber experiments in which they exposed residential biomass burning emissions from a residential wood stove to NO_2 and O_3 under different RH conditions. Here, we compare the produced OA from a medium RH (approximately 45%) experiment with those of the ambient perturbation experiments that had similar RH. The θ angle between the produced OA from perturbation Exp.1 and the one from the laboratory chamber experiment was 11 degrees, indicating a considerable degree of similarity (~~Fig.~~Figure 6). The comparison of our results with the work of Kodros et al. (2020) can also be viewed as an independent test of the validity of our assumption that most of the SOA formed in our experiments was indeed due to biomass burning. This ~~latter~~ previous study used only biomass burning emissions therefore there is no doubt that their results represent bbSOA. The good comparison of the produced SOA spectra in the two studies both strengthens our argument that we mainly observe bbSOA formation and also strengthens the argument of Kodros et al. (2020) that their laboratory results are a reasonable representation of realistic atmospheric processing of biomass burning emissions.

The produced OA was also compared with the ambient oxygenated organic aerosol (OOA) factor identified from the PMF analysis of the ambient data. The θ angle between the ambient OOA in Patras from winter 2020 and the produced OA from Exp. 1 was 10 degrees. Similarities were also observed in the produced OA and OOA from cities around the world during winter periods. For Exp. 1 the θ angle was in the range of 9-18 degrees (Table S2) when compared with OOA factors from Fresno, US (Ge et al., 2012), Barcelona, Spain (Mohr et al., 2012), Paris, France (Crippa et al., 2013), Bologna, Italy (Gilardoni et al., 2016), Athens, Greece (Florou et al., 2017) and Xi'an/Beijing, China (Elser et al., 2016). The contribution of biomass burning ~~in~~to the measured OA in the above field studies~~cities we compared~~ ranged from 16% (Fresno, California) up to 70% (Patras and Athens, Greece) ~~of the OA~~. The OOA as viewed by the PMF analysis of the AMS spectra has most of the time little information about its source. Therefore, this similarity

just strengthens our argument that the SOA produced in our experiments was rather realistic. We further compared the AMS spectrum of the SOA produced in this study with the spectra of the SOA produced during daytime oxidation of biomass burning emissions. There are notable differences in the two spectra, with theta angles approaching 30 degrees. This result is consistent with the findings of Kodros et al. (2020).

3.3 Results of other experiments

The rapid OA production observed during Exp. 1 was also observed in all the other experiments, with approximately 75% of the produced OA formed in the first hour after the ozone injection. The injected ozone levels in the other experiments, excluding Exp. 1 ranged from 65 to 220 ppb. Figure 7 ~~represents~~shows the produced OA (including organic nitrates) in all the perturbation experiments. In all experiments, the majority of secondary ~~nitrate~~ aerosol nitrate ~~was~~were organonitrate, representing 55-85% of the total produced nitrate. Taking into account the organic nitrates, the initial SOA formation rate in the perturbed chamber in the conducted experiments was on average 10 $\mu g\ m^{-3}\ h^{-1}$, ranging from 1 to 30 $\mu g\ m^{-3}\ h^{-1}$.

An increase in the O:C in the perturbed chamber was observed in all experiments with an average increase from the initial O:C of 45% ~~(Table S3 summarizes the OA enhancement and the initial and final O:C in the perturbed chamber in the conducted experiments).~~ At the same time, the O:C in the control chamber remained within 6% of the initial value. Table S3 summarizes the OA enhancement and the initial and final O:C in the perturbed chamber in the conducted experiments.

The mass spectra of the produced OA in the perturbed chamber were similar to that of Exp.1 with the major m/z values being 28, 29, 43, 44, 55 and 69 (Figure 5). The θ angle between the different produced OA spectra in the perturbed experiments were less than 14 degrees, suggesting similarities between the produced OA from the different perturbation experiments. The θ angle between the produced OA mass spectra in the perturbed chamber and the one from Kodros et al. (2020) was in the range of 9-16 degrees, suggesting similarity of the results of the two studies, even if one relied on a single fuel burned in a single stove and the other in a mixture of emissions from ~~hundreds~~ thousands of fireplaces and heating stoves. Another possible explanation of the difference between the two ~~studies~~works is the presence of non-~~biomass burning~~BB emissions in the urban ambient air that could contribute to the SOA formation.

402

403

4.1 Secondary organic aerosol production

The rapid OA production observed during Exp. 1 was also observed in all the other experiments, with approximately 75% of the produced OA formed in the first hour after the ozone injection. Figure 7 represents the produced OA (including organic nitrates) in all the perturbation experiments. In all experiments, the majority of secondary nitrate aerosol were organonitrate, representing 55-85% of the total produced nitrate. Taking into account the organic nitrates, the initial OA formation rate in the perturbed chamber in the conducted experiments was on average 10 $\mu g\ m^{-3}\ h^{-1}$ ranging from 1 to 30 $\mu g\ m^{-3}\ h^{-1}$.

An increase in the O:C in the perturbed chamber was observed in all experiments with an average increase from the initial O:C of 45%. At the same time the O:C in the control chamber remained within 6% of the initial value.

The mass spectra of the produced OA in the perturbed chamber were similar to that of Exp.1 with the major m/z values being 28, 29, 43, 44, 55 and 69 (Fig. 5). The θ angle between the different produced OA spectra in the perturbed experiments were less than 14 degrees, suggesting similarities between the produced OA from the different perturbation experiments. The θ angle between the produced OA mass spectra in the perturbed chamber and the one from Kodros et al. (2020) was in the range of 9-16 degrees, suggesting similarity of the results of the two studies, even if one relied on a single fuel burned in a single stove and the other in a mixture of emissions from hundreds of fireplaces and heating stoves.

4.2 3.4 NO₃ and OH radical levels

Based on the decay of d9-butanol after the injection of ozone, the OH concentration was in the range of 0.2-0.4×10^6 molecules cm^{-3} in the perturbation chamber suggesting that the addition of ozone and reactions with organic vapors were not producing significant OH levels. Given the sunlight in Greece even during the winter, these mentioned levels correspond to less than 10% of the daytime levelsOH in the area during that wintertime period. Despite the relatively low OH in the perturbation chamber, its corresponding reactions with the various VOCs present do contribute to the observed chemical changes. Since the air we are using is a mixture of BB and non-BBVOC

some organic vapors could possibly react with the OH radicals. The characteristic reaction times with the OH of some of the VOCs present (toluene, xylenes, isoprene, monoterpenes and phenol) that could contribute to SOA formation with OH at these levels for some of the VOCS (toluene, xylenes, isoprene, monoterpenes and phenol) ranged from approximately 9 to 160 hours suggesting that these reaction had a small contribution to the rapid SOA formation observed during the first 30 min of a typical experiment (Figure 1). The corresponding OH concentrations are practically negligible in the duration of a typical experiment (4-5 hours). The indirect measurement of the OH levels in the chambers through the decay of d-butanol, showed that through the experiment the OH levels were low and Insteady. iIn the control chamber the corresponding OH concentrations were practically zero and below the detection levels of the d9-butanol approach, since no additional ozone was added that could react with the organic vapors and produce OH. Measurements of the OH levels were only possible when the PTR-MS was available (Exps 9-11), but the results were pretty consistent. Some OH production is also expected in the ambient atmosphere as the ozone mixes in the nighttime boundary layer from aloft, so these reactions are also taking place, albeit slowly, in the ambient atmosphere too.

Nitrate radical concentrations above the detection level of a few ppt were only measured in the perturbed chamber after the ozone injection. The maximum NO_3 radical concentrations in the perturbed chamber ranged from 3 to 25 ppt with the highest observed during Exp. 8 (Table S3). In this experiment before the ozone injection the NO_3 levels in both chambers were below the detection limit of the instrument, while after the injection (t=0 h) the concentration of NO_3 started to increase (Fig.Figure S44). In Exp. 8 there were 44 ppb of NO_x initially and 150 ppb of O_3 were injected. Approximately 15 µg m^{-3} of OA was formed in 2.5 h after the perturbation, with close to 2 µg m^{-3} of the OA formed being organic nitrate. The O:C reached a value of 0.6 at the end of this experiment.

The measured NO_3 concentrations along with the low concentrations of OH in the perturbed chamber suggests that the reactions of VOCs with NO_3 radicals and potentially ozone were the major source of SOA production.

4.3 3.5 Factors affecting the SOA production

The highest produced SOA was observed, as expected, in experiments that had high initial OA and VOC levels and therefore took place during polluted conditions. Experiments 1, 4 and 6

had the highest measured inital VOC levels among the conducted experiments, close to 150 μg m^{-3} (Table 1Fig.Figure S2). Although, only a fraction of the VOCs present in the atmosphere were measured by the PTR-MS in this work, these measurements provide an indication of the SOA formation potential of the corresponding air masses. We could identify not find a strong link between the small variations in the speciation of the initial VOCs and the SOA formed. This is probably due to the fact that we only quantified only a small fraction of the VOCs and IVOCs that serve as SOA precursors in the system.

The absolute concentration of SOA formed was also affected by the levels of NO present. Experiments with low initial NO, less than 5 ppb, (Experiments 2, 3, 5 ,9 and 11) had the lowest SOA production. The lowest NO_3 radical concentrations were also observed in those experiments. This is due to the low NO_x availability in the atmosphere during these experiments. These low NO_x levels result in low NO_3 levels in the perturbed chamber and therefore together with the relatively low VOC levels, during the same daysperiods, lead to low SOA production. Figure 8 shows the correlation between the concentration of NO_3 radicals and the produced organic nitrate levels in the perturbed chamber. The good correlation (R^2=0.79) supports the strong link between the NO_3 chemistry occurring in the perturbed chamber and the corresponding SOA production. This suggests that the oxidants levels (mainly NO_3) produced after reactions of ozone with the pre-existing NO_x are affecting significantly the levels of SOA formed under these conditions. We estimated an R^2=0.66 between the formed SOA and the levels of NO_3 in the perturbed chamber (Figure S5).

5 4. Conclusions

In this work, we studied the nighttime aging of urban wintertime air, strongly influenced by biomass burning emissions in Patras, Greece. Using a dual chamber system and ambient air as a starting point, we injected additional ozone in only one chamber to accelerate nitrate radical production via reactions with the pre-existing NO_x. The other chamber was used as a reference mainly as a safeguard against potential experimental artifacts. The novelty of this techniqueexperimental approach is that it allowed the quantification of the nighttime chemical transformations of realistic biomass burning emissions from thousands of sources and multiple fuels after they had been diluted and mixed with ambient air. is that allows the further study of oxidation of realistic air. Our study has been designed so that the Our eexperiments took place

during periods in which biomass burning was responsible for 70% on average of the ambient OA and therefore the biomass burning emissions were the dominant source of VOCs and IVOCs. ~~start when biomass burning is the major source of both organic aerosol and VOCs.~~

After the addition of ozone, rapid SOA formation was observed in the perturbed chamber with the additional OA formed reaching up to 35 μg m^{-3}. The SOA formed increased the pre-existing OA by 20-70%. Most of the secondary nitrate formed was ~~attributed to~~ organic nitrate~~s~~, in some cases reaching up to 85% of the total aerosol nitrate. On average 10% of the total OA formed was organic nitrate. The organic aerosol formation was rapid, with 75% of the produced OA formed in the first hour after the ozone injection. The organic aerosol content in the control chamber remained within 10% of the initial ~~injected~~ levels, suggesting limited chemical oxidation without the addition of ozone in these timescales. These results strongly suggest that significant secondary OA can be formed even during the nighttime of winter periods through the chemical processing of biomass burning emissions.

The O:C of organic aerosol increased rapidly in the perturbed chamber following the ozone injection. In 2-3 h of reactions a 40-50% increase of the O:C was observed while the OA O:C in the control chamber remained within approximately 5% of the initial value. The produced OA mass spectra showed similarities with the produced OA factor from ~~a previous~~ dark aging biomass burning experiments under laboratory conditions, pointing towards the important role of biomass burning emissions in the OA formed in a winter urban environment. Furthermore, the produced SOA mass spectra were quite similar to those of ambient oxygenated OA factors found in urban areas during winter periods in which the fresh bbOA contributed 15-70% of the OA.

Nitrate radicals were observed only in the perturbed chamber and only after the ozone injection. Their levels reached up to 25 ppt. ~~Along with the~~The low and steady levels of hydroxyl radical in the perturbed chamber along with the high characteristic reactions times of the measured VOCs with the OH compared to the duration of the experiments, indicates that reaction with nitrate radicals and ozone were responsible for the SOA formation and the change in the OA composition.

Author Contribution: S.D.J., K.F., C.K., J.K.K. and C.V. conducted the experiments, collected and analyzed the data. S.N.P and A.N. conceived and directed the study. M.C., A.F. and B.P.-V. provided the IBB-CEAS. S.D.J. and S.N.P. wrote the manuscript with inputs from all co-authors.

526 *Data availability*: Data related to this article are available upon request to the corresponding author.

527 The data will be available in the EUROCHAMP-2020 website.

528

529 *Competing interests*: The authors declare that they have no conflict of interest.

530

531 **Acknowledgements**

532 This work was supported by the European Union's Horizon 2020 EUROCHAMP–2020

533 Infrastructure Activity (grant agreement 730997) and project PyroTRACH (ERC-2016-COG)

534 funded from H2020-EU.1.1. - Excellent Science - European Research Council (ERC), project ID

535 726165. We thank Prof. A. Papalou and the University of Peloponnese for providing the space for

536 our experiments.

537

538 **References**

539 Ahern, A. T., Robinson, E. S., Tkacik, D. S., Saleh, R., Hatch, L. E., Barsanti, K. C., Stockwell,

540   C. E., Yokelson, R. J., Presto, A. A., Robinson, A. L., Sullivan, R. C. and Donahue, N. M.:

541   Production of secondary organic aerosol during aging of biomass burning smoke from

542   fresh fuels and its relationship to VOC precursors, J. Geophys. Res., 124, 3583–3606, 2019.

543 Akagi, S. K., Yokelson, R. J., Wiedinmyer, C., Alvarado, M. J., Reid, J. S., Karl, T., Crounse, J.

544   D. and Wennberg, P. O.: Emission factors for open and domestic biomass burning for use

545   in atmospheric models, Atmos. Chem. Phys., 11, 4039–4072, 2011.

546 Akherati, A., He, Y., Coggon, M. M., Koss, A. R., Hodshire, A. L., Sekimoto, K., Warneke, C.,

547   De Gouw, J., Yee, L., Seinfeld, J. H., Onasch, T. B., Herndon, S. C., Knighton, W. B.,

548   Cappa, C. D., Kleeman, M. J., Lim, C. Y., Kroll, J. H., Pierce, J. R. and Jathar, S. H.:

549   Oxygenated aromatic compounds are important precursors of secondary organic aerosol in

550   biomass-burning emissions, Environ. Sci. Technol., 54, 8568–8579, 2020.

551 Alfarra, M. R., Prevot, A. S. H., Szidat, S., Sandradewi, J., Weimer, S., Lanz, V. A., Schreiber, D.,

552   Mohr, M. and Baltensperger, U.: Identification of the mass spectral signature of organic

553   aerosols from wood burning emissions, Environ. Sci. Technol., 41, 5770–5777, 2007.

554 Andreae, M. O. and Merlet, P.: Emission of trace gases and aerosols from biomass burning, Global

555   Biogeochem. Cycles, 15, 955–966, 2001.

556 Bond, T. C., Streets, D. G., Yarber, K. F., Nelson, S. M., Woo, J. H. and Klimont, Z.: A technology-
557   based global inventory of black and organic carbon emissions from combustion, J.
558   Geophys. Res., 109, D14203, doi:10.1029/2003JD003697, 2004.

559 Bougiatioti, A., Stavroulas, I., Kostenidou, E., Zarmpas, P., Theodosi, C., Kouvarakis, G.,
560   Canonaco, F., Prévôt, A. S. H., Nenes, A., Pandis, S. N. and Mihalopoulos, N.: Processing
561   of biomass-burning aerosol in the eastern Mediterranean during summertime, Atmos.
562   Chem. Phys., 14, 4793–4807, 2014.

563 Boy, J., Rollenbeck, R., Valarezo, C. and Wilcke, W.: Amazonian biomass burning-derived acid
564   and nutrient deposition in the north Andean montane forest of Ecuador, Global
565   Biogeochem. Cycles, 22, GB4011, 2008.

566 Brown, S. S., deGouw, J. A., Warneke, C., Ryerson, T. B., Dubé, W. P., Atlas, E., Weber, R. J.,
567   Peltier, R. E., Neuman, J. A., Roberts, J. M., Swanson, A., Flocke, F., McKeen, S. A.,
568   Brioude, J., Sommariva, R., Trainer, M., Fehsenfeld, F. C., and Ravishankara, A. R.:
569   Nocturnal isoprene oxidation over the Northeast United States in summer and its impact
570   on reactive nitrogen partitioning and secondary organic aerosol, Atmos. Chem. Phys., 9,
571   3027–3042, 2009

572 Brown, S. S., Dubé, W. P., Bahreini, R., Middlebrook, A. M., Brock, C. A., Warneke, C., de Gouw,
573   J. A., Washenfelder, R. A., Atlas, E., Peischl, J., Ryerson, T. B., Holloway, J. S., Schwarz,
574   J. P., Spackman, R., Trainer, M., Parrish, D. D., Fehshenfeld, F. C., and Ravishankara, A.
575   R.: Biogenic VOC oxidation and organic aerosol formation in an urban nocturnal boundary
576   layer: aircraft vertical profiles in Houston, TX, Atmos. Chem. Phys., 13, 11317–11337,
577   2013.

578 Bruns, E. A., El Haddad, I., Slowik, J. G., Kilic, D., Klein, F., Baltensperger, U. and Prévôt, A. S.
579   H.: Identification of significant precursor gases of secondary organic aerosols from
580   residential wood combustion, Sci. Rep., 6, 27881, 2016.

581 Canagaratna, M. R., Jimenez, J. L., Kroll, J. H., Chen, Q., Kessler, S. H., Massoli, P., Hildebrandt
582   Ruiz, L., Fortner, E., Williams, L. R., Wilson, K. R., Surratt, J. D., Donahue, N. M., Jayne,
583   J. T. and Worsnop, D. R.: Elemental ratio measurements of organic compounds using
584   aerosol mass spectrometry: characterization, improved calibration, and implications,
585   Atmos. Chem. Phys., 15, 253–272, 2015.

586 Capes, G., Johnson, B., McFiggans, G., Williams, P. I., Haywood, J. and Coe, H.: Aging of
587   biomass burning aerosols over West Africa: Aircraft measurements of chemical
588   composition, microphysical properties, and emission ratios, J. Geophys. Res., 113, 1–13,
589   2008.

590 Crippa, M., DeCarlo, P. F., Slowik, J. G., Mohr, C., Heringa, M. F., Chirico, R., Poulain, L.,
591   Freutel, F., Sciare, J., Cozic, J., Di Marco, C. F., Elsasser, M., Nicolas, J. B., Marchand,
592   N., Abidi, E., Wiedensohler, A., Drewnick, F., Schneider, J., Borrmann, S., Nemitz, E.,
593   Zimmermann, R., Jaffrezo, J.-L., Prévôt, A. S. H. and Baltensperger, U.: Wintertime
594   aerosol chemical composition and source apportionment of the organic fraction in the
595   metropolitan area of Paris, Atmos. Chem. Phys., 13, 961–981, 2013.

596 Decker, Z. C. J., Zarzana, K. J., Coggon, M., Min, K. E., Pollack, I., Ryerson, T. B., Peischl, J.,
597   Edwards, P., Dubé, W. P., Markovic, M. Z., Roberts, J. M., Veres, P. R., Graus, M.,
598   Warneke, C., De Gouw, J., Hatch, L. E., Barsanti, K. C. and Brown, S. S.: Nighttime
599   chemical transformation in biomass burning plumes: A box model analysis initialized with
600   aircraft observations, Environ. Sci. Technol., 53, 2529–2538, 2019.

601 Elser, M., Huang, R.-J., Wolf, R., Slowik, J. G., Wang, Q., Canonaco, F., Li, G., Bozzetti, C.,
602   Daellenbach, K. R., Huang, Y., Zhang, R., Li, Z., Cao, J., Baltensperger, U., El-Haddad, I.
603   and Prévôt, A. S. H.: New insights into $PM_{2.5}$ chemical composition and sources in two
604   major cities in China during extreme haze events using aerosol mass spectrometry, Atmos.
605   Chem. Phys., 16, 3207–3225, 2016.

606 Farmer, D. K., Matsunaga, A., Docherty, K. S., Surratt, J. D., Seinfeld, J. H., Ziemann, P. J. and
607   Jimenez, J. L.: Response of an aerosol mass spectrometer to organonitrates and
608   organosulfates and implications for atmospheric chemistry, Proc. Natl. Acad. Sci.., 107,
609   6670–6675, 2010.

610 Favez, O., El Haddad, I., Piot, C., Boréave, A., Abidi, E., Marchand, N., Jaffrezo, J.-L., Besombes,
611   J.-L., Personnaz, M.-B., Sciare, J., Wortham, H., George, C. and D'Anna, B.: Inter-
612   comparison of source apportionment models for the estimation of wood burning aerosols
613   during wintertime in an Alpine city (Grenoble, France), Atmos. Chem. Phys., 10, 5295–
614   5314, 2010.

615 Florou, K., Papanastasiou, D. K., Louvaris, E., Kaltsonoudis, C., Patoulias, D., Pikridas, M.,
616   Gkatzelis, G. I., Pandis, S. N. and Mihalopoulos, N.: The contribution of wood burning and

617   other pollution sources to wintertime organic aerosol levels in two Greek cities, Atmos.

618   Chem. Phys., 17, 3145–3163, 2017.

619   Ford, B., Val Martin, M., Zelasky, S. E., Fischer, E. V., Anenberg, S. C., Heald, C. L. and Pierce,

620   J. R.: Future fire impacts on smoke concentrations, visibility, and health in the contiguous

621   United States, GeoHealth, 2, 229–247, 2018.

622   Fouqueau, A., Cirtog, M., Cazaunau, M., Pangui, E., Zapf, P., Siour, G., Landsheere, X., Méjean,

623   G., Romanini, D., and Picquet-Varrault, B.: Implementation of an incoherent broadband

624   cavity-enhanced absorption spectroscopy technique in an atmospheric simulation chamber

625   for in situ NO3 monitoring: characterization and validation for kinetic studies, Atmos.

626   Meas. Tech., 13, 6311–6323, 2020.

627   Fountoukis, C., Megaritis, A. G., Skyllakou, K., Charalampidis, P. E., Denier van der Gon, H. A.

628   C., Crippa, M., Prévôt, A. S. H., Fachinger, F., Wiedensohler, A., Pilinis, C. and Pandis, S.

629   N.: Simulating the formation of carbonaceous aerosol in a European Megacity (Paris)

630   during the MEGAPOLI summer and winter campaigns, Atmos. Chem. Phys., 16, 3727–

631   3741, 2016.

632   Fuller, G. W., Tremper, A. H., Baker, T. D., Yttri, K. E. and Butterfield, D.: Contribution of wood

633   burning to PM10 in London, Atmos. Environ., 87, 87–94, 2014.

634   Ge, X., Setyan, A., Sun, Y. and Zhang, Q.: Primary and secondary organic aerosols in Fresno,

635   California during wintertime: Results from high resolution aerosol mass spectrometry, J.

636   Geophys. Res., 117, D19301, doi:10.1029/2012JD018026, 2012.

637   Gilardoni, S., Massoli, P., Paglione, M., Giulianelli, L., Carbone, C., Rinaldi, M., Decesari, S.,

638   Sandrini, S., Costabile, F., Gobbi, G. P., Pietrogrande, M. C., Visentin, M., Scotto, F.,

639   Fuzzi, S. and Facchini, M. C.: Direct observation of aqueous secondary organic aerosol

640   from biomass-burning emissions, Proc. Natl. Acad. Sci., 113, 10013–10018, 2016.

641   Hartikainen, A., Yli-Pirilä, P., Tiitta, P., Leskinen, A., Kortelainen, M., Orasche, J., Schnelle-

642   Kreis, J., Lehtinen, K. E. J., Zimmermann, R., Jokiniemi, J. and Sippula, O.: Volatile

643   organic compounds from logwood combustion: Emissions and transformation under dark

644   and photochemical aging conditions in a smog chamber, Environ. Sci. Technol., 52, 4979–

645   4988, 2018.

646   Hennigan, C. J., Miracolo, M. A., Engelhart, G. J., May, A. A., Presto, A. A., Lee, T., Sullivan, A.

647   P., McMeeking, G. R., Coe, H., Wold, C. E., Hao, W.-M., Gilman, J. B., Kuster, W. C., de

Gouw, J., Schichtel, B. A., Collett, J. L., Kreidenweis, S. M. and Robinson, A. L.: Chemical and physical transformations of organic aerosol from the photo-oxidation of open biomass burning emissions in an environmental chamber, Atmos. Chem. Phys., 11, 7669–7686, 2011.

Jolleys, M. D., Coe, H., McFiggans, G., Taylor, J. W., O'Shea, S. J., Le Breton, M., Bauguitte, S. J.-B., Moller, S., Di Carlo, P., Aruffo, E., Palmer, P. I., Lee, J. D., Percival, C. J. and Gallagher, M. W.: Properties and evolution of biomass burning organic aerosol from Canadian boreal forest fires, Atmos. Chem. Phys., 15, 3077–3095, 2015.

Jorga, S. D., Kaltsonoudis, C., Liangou, A. and Pandis, S. N.: Measurement of formation rates of secondary aerosol in the ambient urban atmosphere using a dual smog chamber system, Environ. Sci. Technol., 54, 1336–1343, 2020.

Kaltsonoudis, C., Jorga, S. D., Louvaris, E., Florou, K. and Pandis, S. N.: A portable dual-smog-chamber system for atmospheric aerosol field studies, Atmos. Meas. Tech., 12, 2733–2743, 2019.

Kodros, J. K., Papanastasiou, D. K., Paglione, M., Masiol, M., Squizzato, S., Florou, K., Skyllakou, K., Kaltsonoudis, C., Nenes, A. and Pandis, S. N.: Rapid dark aging of biomass burning as an overlooked source of oxidized organic aerosol, Proc. Natl. Acad. Sci., 52, 33028-33033, 2020.

Kostenidou, E., Pathak, R. K. and Pandis, S. N.: An algorithm for the calculation of secondary organic aerosol density combining AMS and SMPS data, Aerosol Sci. Technol., 41, 1002–1010, 2007.

Kostenidou, E., Lee, B. H., Engelhart, G. J., Pierce, J. R. and Pandis, S. N.: Mass spectra deconvolution of low, medium, and high volatility biogenic secondary organic aerosol, Environ. Sci. Technol., 43, 4884–4889, 2009.

Mohr, C., DeCarlo, P. F., Heringa, M. F., Chirico, R., Slowik, J. G., Richter, R., Reche, C., Alastuey, A., Querol, X., Seco, R., Peñuelas, J., Jiḿenez, J. L., Crippa, M., Zimmermann, R., Baltensperger, U. and Prév̂ot, A. S. H.: Identification and quantification of organic aerosol from cooking and other sources in Barcelona using aerosol mass spectrometer data, Atmos. Chem. Phys., 12, 1649–1665, 2012.

O'Dell, K., Ford, B., Fischer, E. V. and Pierce, J. R.: Contribution of Wildland-Fire Smoke to US PM 2.5 and Its Influence on Recent Trends, Environ. Sci. Technol., 53, 1797–1804, 2019.

679 Orphal, J., Fellows, C. E., and Flaud, P.-M.: The visible absorption spectrum of NO_3 measured by
680   high-resolution Fourier transform spectroscopy, J. Geophys. Res., 108, 4077,
681   doi:10.1029/2002JD002489, 2003.

682 Ortega, A. M., Day, D. A., Cubison, M. J., Brune, W. H., Bon, D., De Gouw, J. A. and Jimenez,
683   J. L.: Secondary organic aerosol formation and primary organic aerosol oxidation from
684   biomass-burning smoke in a flow reactor during FLAME-3, Atmos. Chem. Phys., 13,
685   11551–11571, 2013.

686 Robinson, A. L., Subramanian, R., Donahue, N. M., Bernardo-Bricker, A. and Rogge, W. F.:
687   Source apportionment of molecular markers and organic aerosol. 2. Biomass smoke,
688   Environ. Sci. Technol., 40, 7811–7819, 2006.

689 Sundarambal, P., Balasubramanian, R., Tkalich, P. and He, J.: Impact of biomass burning on
690   Ocean water quality in Southeast Asia through atmospheric deposition: Field observations,
691   Atmos. Chem. Phys., 10, 11323–11336, 2010.

692 Tkacik, D. S., Robinson, E. S., Ahern, A., Saleh, R., Stockwell, C., Veres, P., Simpson, I. J.,
693   Meinardi, S., Blake, D. R., Yokelson, R. J., Presto, A. A., Sullivan, R. C., Donahue, N. M.
694   and Robinson, A. L.: A dual-chamber method for quantifying the effects of atmospheric
695   perturbations on secondary organic aerosol formation from biomass burning emissions, J.
696   Geophys. Res., 122, 6043–6058, 2017.

697 Tsimpidi, A. P., Karydis, V. A., Pozzer, A., Pandis, S. N. and Lelieveld, J.: ORACLE (v1.0):
698   module to simulate the organic aerosol composition and evolution in the atmosphere,
699   Geosci. Model Dev., 7, 3153–3172, 2014.

700 Vakkari, V., Beukes, J. P., Dal Maso, M., Aurela, M., Josipovic, M. and van Zyl, P. G.: Major
701   secondary aerosol formation in southern African open biomass burning plumes, Nat.
702   Geosci., 11, 580–583, 2018.

703 Vandaele, A. C., Hermans, C., Simon, P. C., Carleer, M., Colin, R., Fally, S., Mérienne, M. F.,
704   Jenouvrier, A., and Coquart, B.: Measurements of the NO_2 absorption cross-section from
705       $42\,000\,cm^{-1}$ to $10\,000\,cm^{-1}$ (238–1000 nm) at 220K and 294 K., J. Quant. Spectrosc. Radiat.
706   Transf., 59, 171–184, 1998.

707 Wang, N., Jorga, S. D., Pierce, J. R., Donahue, N. M. and Pandis, S. N.: Particle wall-loss
708   correction methods in smog chamber experiments, Atmos. Meas. Tech., 11, 6577–6588,
709   2018.

710   Watson, J. G.: Visibility: Science and regulation, J. Air Waste Manag. Assoc., 52, 628–713, 2002.

711   Yu, J., Cocker, D. R., Griffin, R. J., Flagan, R. C. and Seinfeld, J. H.: Gas-phase ozone oxidation

712   of monoterpenes: Gaseous and particulate products, J. Atmos. Chem., 34, 207–258, 1999.

713   Zhao, D. F., Kaminski, M., Schlag, P., Fuchs, H., Acir, I.-H., Bohn, B., Häseler, R., Kiendler-

714   Scharr, A., Rohrer, F., Tillmann, R., Wang, M. J., Wegener, R., Wildt, J., Wahner, A. and

715   Mentel, T. F.: Secondary organic aerosol formation from hydroxyl radical oxidation and

716   ozonolysis of monoterpenes, Atmos. Chem. Phys., 15, 991–1012, 2015.

717

718

719

720

721

722

723

724

725

726   **Table 1:** Initial conditions for the dual chamber experiments.

Exp.	Start Time (LT)	RH (%)	Temperature (°C)	BC (µg m^{-3})	OA (µg m^{-3})	% bbBB OA	O:C	NO (ppb)	NO$_2$ (ppb)	Total VOCs[b] (µg m^{-3})
1	17:45	45	17	2.4	44	70	0.4	17	24	150
2	17:45	35	13	0.8	18	65	0.36	4	22	50
3	17:50	33	15	0.6	19	37	0.25	3	20	38
4	17:55	40	14	2.5	48	68	0.33	90	20	160
5	17:45	35	15	1.1	18	69	0.4	3	25	71
6	17:50	40	17	2.6	50	72	0.36	32	25	160
7	18:00	45	20	1.0	16	78	0.36	15	20	63

8	17:55	42	22	1.2	22	77	0.45	22	22	75
9	18:15	40	19	0.7	16	75	0.44	3	14	46
10	18:15	45	21	1.6	25	50	0.33	32	21	100
11	18:30	45	24	0.6	6	48	0.41	1	5	38
12[a]	18:00	32	21	2.1	6	65	0.37	3	15	131
13[a]	18:20	30	19	3.0	33	67	0.35	31	23	188

[a] Blank ~~experiments.~~experiment.
[b] Sum of the VOCs quantified by the PTR-MS.
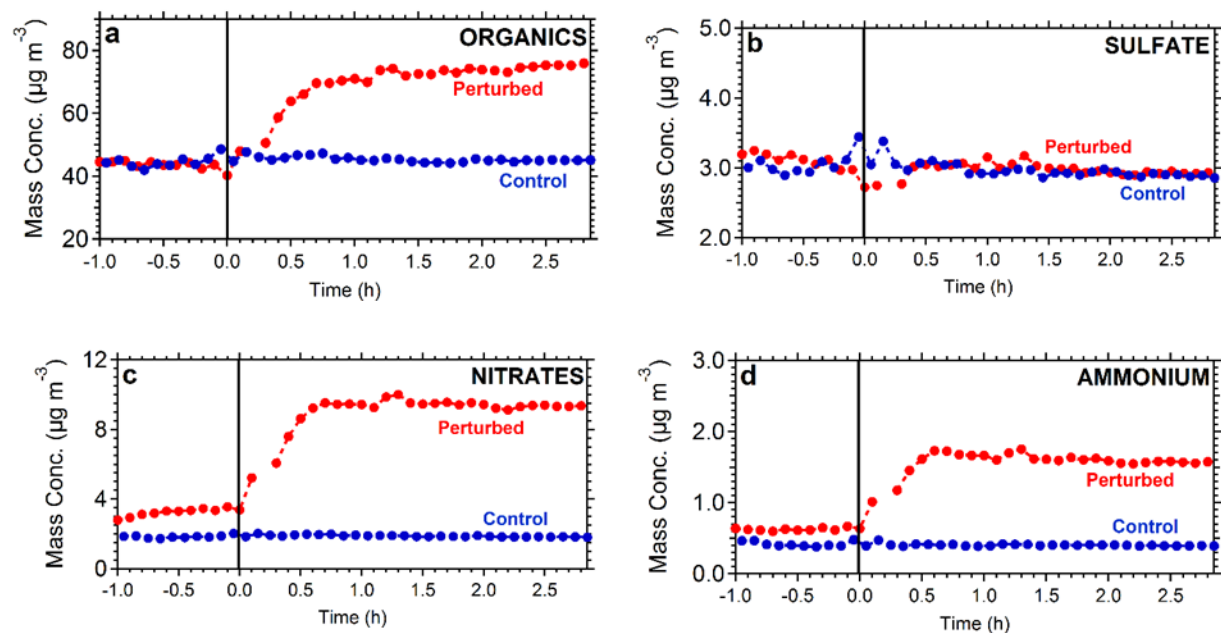
Figure 1: Particle wall-loss corrected aerosol mass concentration (CE=0.4) for the AMS-measured (a) organics, (b) sulfate, (c) nitrates, and (d) ammonium in both the perturbed (red line) and the control chamber (blue line) during Exp. 1.

756
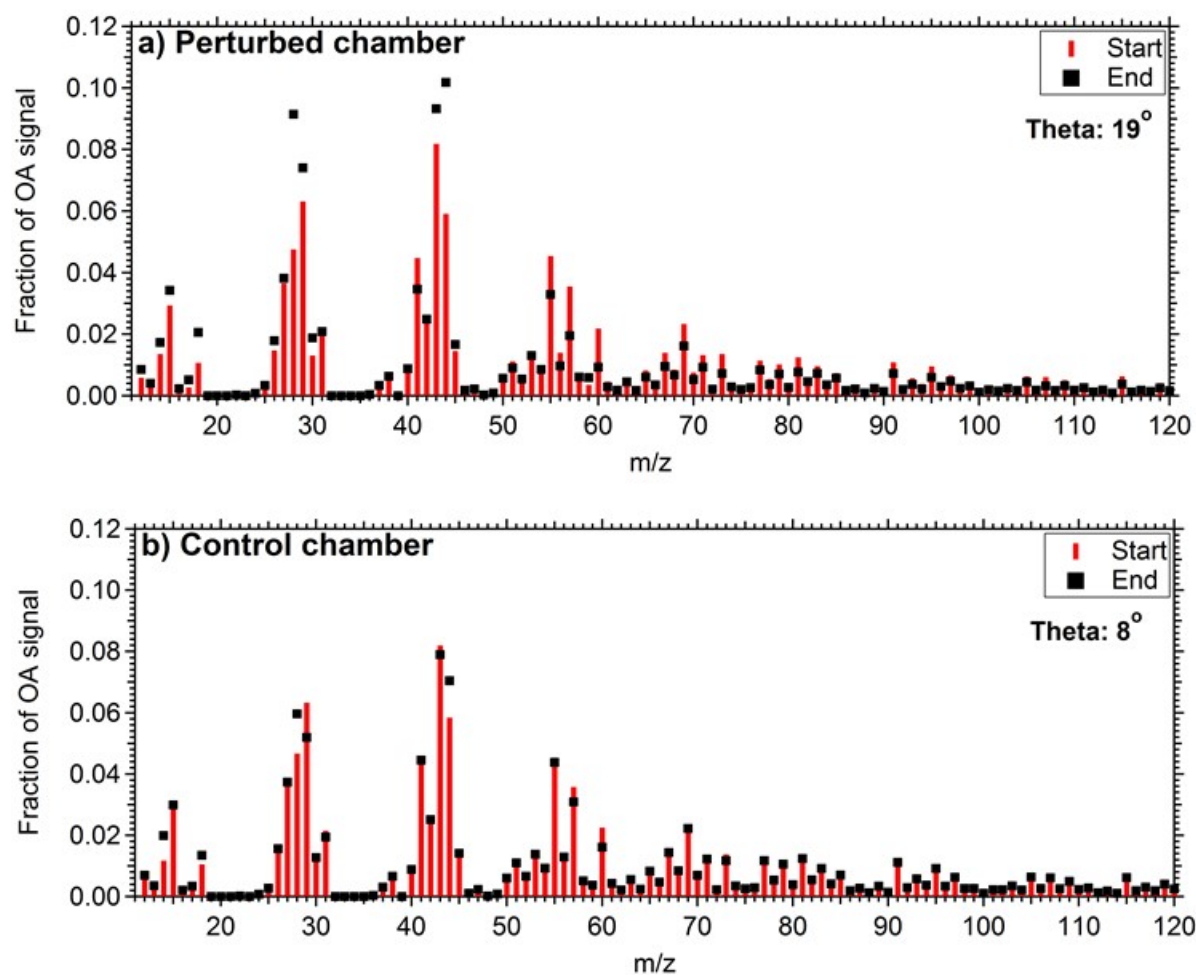
757

758

Figure 2: Mass spectra of OA during Exp. 1 in the (a) perturbed chamber and (b) control chamber
at the start of the experiment (after the filling process) and at the end of the experiment.

761

762

763

764
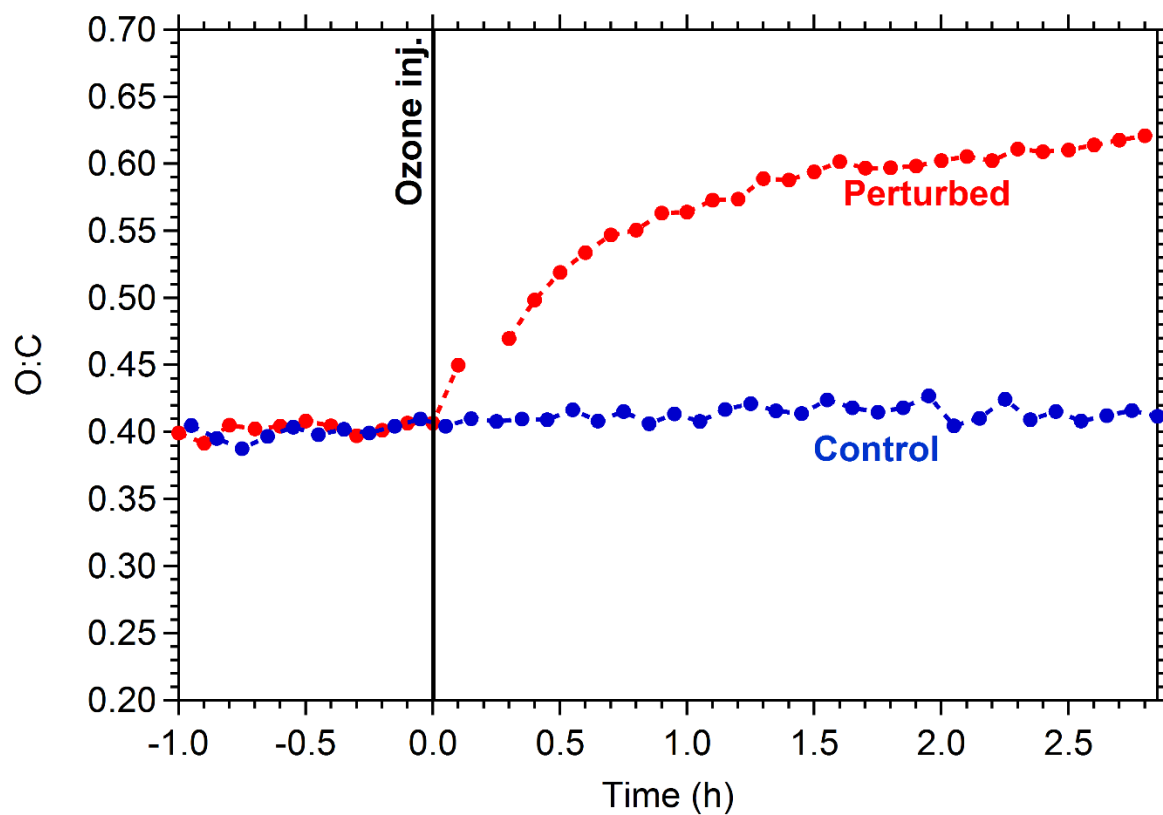
765 **Figure 3:** Oxygen to carbon ratio of the OA in the perturbed (red line) and the control chamber

766 (blue line) during Exp. 1.

767

768

769

770

771

772

773

774

775

776

777

778

779
780
781
782
783

Figure 4: Mass concentration of the measured OA (black points), the initial OA (red points) and the produced SOA (blue points) in the perturbed chamber in Exp. 1. All concentrations refer to the suspended aerosol in the chamber and do not include the material deposited on the chamber walls.

787
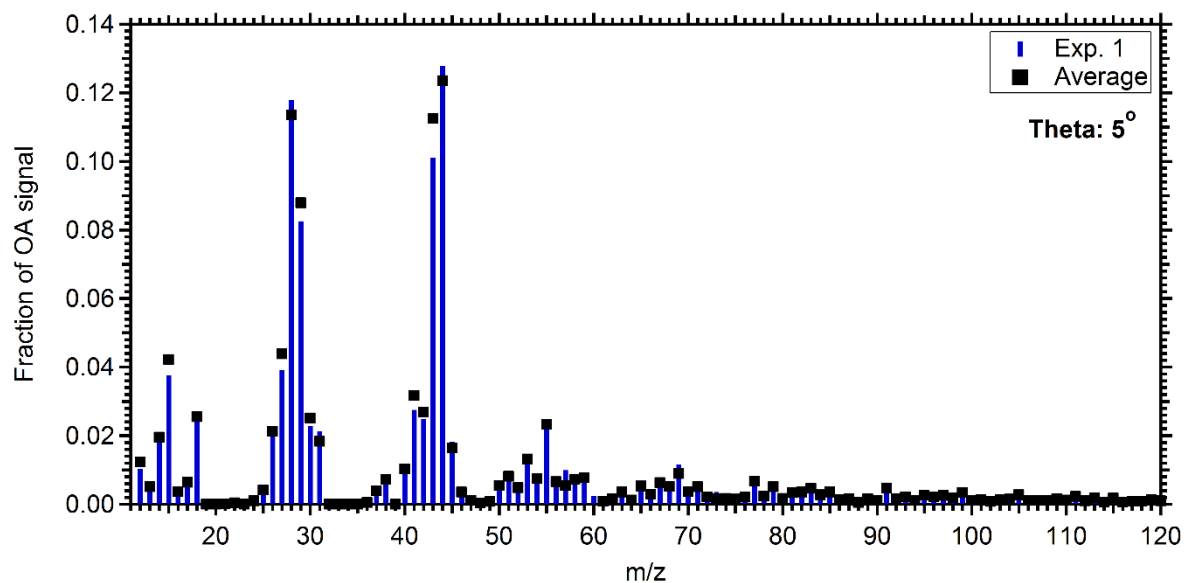
788 **Figure 5:** Mass spectrum of the produced SOA in the perturbed chamber for Exp. 1 (blue bars)

789 and the average spectrum of the produced SOA in all experiments (black squares).

790

791

792

793

794

795

796

797

798

799

800

801

802

803

804

805

806

807

808
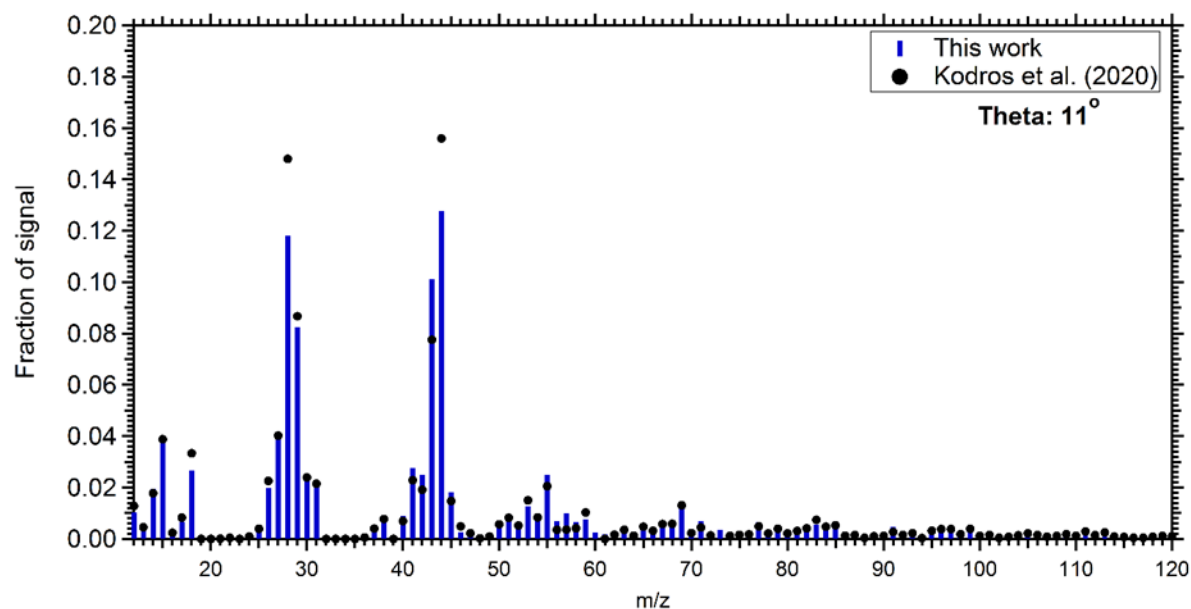
809 **Figure 6:** Comparison of the produced SOA mass spectra in the perturbed chamber during Exp. 1

810 (blue bars) and the produced SOA estimated during the chamber experiments of nocturnal aging

811 of biomass burning emissions (Kodros et al. 2020) (black circles).

812

813

814

815

816

817

818

819

820

821

822

823

824

825

826

827

828
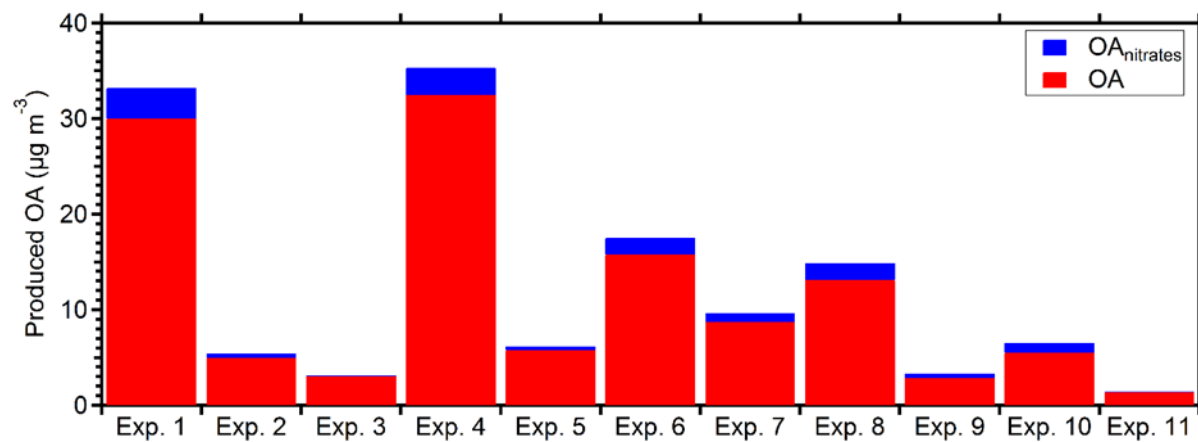
829   **Figure 7:** Produced OA (red bars) and the estimated organic nitrate (blue bars) in the perturbed

830   chamber for the eleven perturbation experiments. All values have been corrected for wall losses

831   and the AMS collection efficiency.

832

833

834

835

836

837

838

839

840

841

842

843

844

845

846

847

848

849
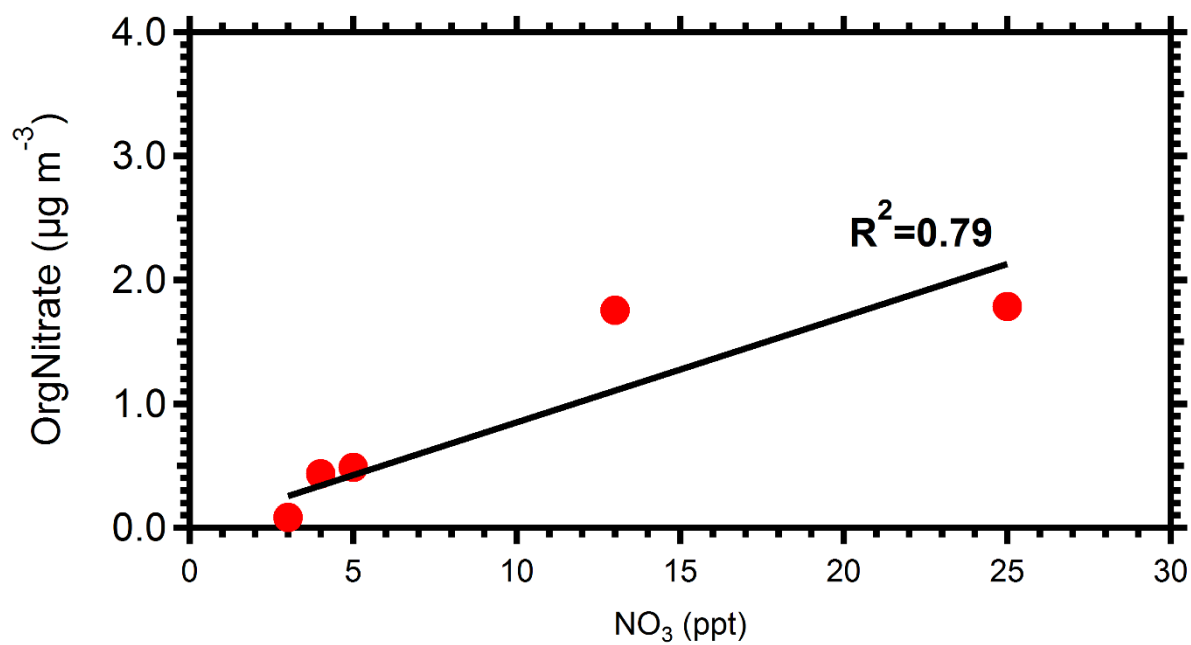
850   **Figure 8**: Correlation between NO_3 radicals with the organic nitrate formed in the perturbed

851   chamber.

852

853

854

855